Journal of Power Sources 199 (2012) 227–238

Contents lists available at SciVerse ScienceDirect

Journal of Power Sources

journal homepage: www.elsevier.com/locate/jpowsour

Electro-thermal modeling and experimental validation for lithium ion battery

Yonghuang Ye[a], Yixiang Shi[a,*], Ningsheng Cai[a], Jianjun Lee[b], Xiangming He[b]

[a] Key laboratory for Thermal Science and Power Engineering of Ministry of Education, Tsinghua University, Beijing 100084, China
[b] Institute of Nuclear and New Energy Technology, Tsinghua University, Beijing 100084, China

ARTICLE INFO

Article history:
Received 12 August 2011
Received in revised form
26 September 2011
Accepted 9 October 2011
Available online 14 October 2011

Keywords:
Lithium ion battery
Heat generation
Lithium ion concentration
Electro-thermal model
Parameter estimation

ABSTRACT

Thermal management is crucial for improving the charge–discharge efficiency and cycling life of lithium ion battery. In this paper, a mathematical model coupling electronic conduction, mass transfer, energy balance and electrochemical mechanism is developed. Lithium ion diffusivity and chemical reaction rate of cathode material are estimated by comparing simulated results with experimental data of pulse test at various current charge–discharge rates (0.2C, 0.5C, 1C, 2C) and operating temperatures (0 °C, 10 °C, 25 °C, 55 °C). The modeling results are further validated in aspects of electrochemical performance, thermal performance and electrochemical-thermal coupling effects, which show well agreement between the modeling results and experimental results. The modeling results show that lithium ion concentration gradient in both liquid phase and solid phase are greatly affected by temperature, and the lithium ion concentration gradient increase when temperature decrease. This phenomenon results in the capacity losses and power loses of lithium ion battery during low temperature operation. The reversible heat generation during charging process is equal with the heat consumption during discharging process. It is also indicated that the reversible heat is dominant at low rate discharging process and irreversible heat is dominant at high rate discharging process. Proper cooling system should be added to keep battery temperature within safety range during high rate current charging/discharging.

1. Introduction

Lithium rechargeable batteries of various types have been moving rapidly toward commercialization ascribing to their potential advantages in power density, cost, safety, performance, or design flexibility. Recently, it has been paid more and more attention to the application on electric vehicle (EV) and hybrid electric vehicle (HEV). The designers need a complete understanding of the characteristics of lithium ion battery [1]. However, choosing among the various chemistries and optimizing the design of battery for a certain application field will be a costly and time-consuming experimental undertaking. Numerical modeling and simulation of the battery is crucial for improving the fundamental understanding of battery operation and for designing appropriate thermal management system.

Several electro-thermal models of lithium ion battery have been presented in published literature. Newman and Pals [2,3] considered isothermal and adiabatic discharge behaviors in the thermal models of cell and battery stack by adding an energy balance equation to the pseudo two dimensional porous electrode models of Doyle et al. [4]. Other researchers [1,5,6] further developed electrochemical-thermal model by adding separated heat source terms and by employing temperature dependent parameters (lithium ion diffusivity, conductivity, etc.). Generally, heat generation within lithium ion battery can be classified into three types: (1) the activation polarization irreversible heat due to the electrochemical reaction polarization between active material particle surface and the electrolyte; (2) ohmic heat due to the ohmic potential drop and (3) reversible reaction heat due to entropy change during charge–discharge.

Furthermore, for a given mathematic model, although most of the model parameters are determined from experiments or from the literature, others are only estimates. Some of the parameters are adjusted to ensure good agreement between the model results and the experimental data, for example kinetic and transport properties. The uncertainty in the estimated parameter will surely influence the model reliability and accuracy. The more the parameters are determined independently through experiments or characterization techniques, the more robust the model. In addition, the comparison between experimental charge and discharge data and modeling results helps battery designer deeply understand the effects of various parameters (thermodynamic, kinetic, and design) on the battery performance with different operating conditions, such as charge–discharge rate and temperature. Thus, the modeling efforts can possibly reduce the experimental work required.

In this study, an electro-thermal coupling model of lithium ion battery is proposed. Model parameters which are sensitive to

* Corresponding author. Tel.: +86 10 62789955; fax: +86 10 62770209.
E-mail address: shyx@tsinghua.edu.cn (Y. Shi).

0378-7753/$ – see front matter © 2011 Elsevier B.V. All rights reserved.
doi:10.1016/j.jpowsour.2011.10.027

Nomenclature

A_{cell}	area of the positive (both sides) that has opposing negative (m^2)
$c_{1,i}$	reduced-lithium in active material ($mol\,m^{-3}$)
$C_{1,max,i}$	maximum concentration ($mol\,m^{-3}$)
$c_{1,surf,i}$	lithium ion concentration on active material particles ($mol\,m^{-3}$)
$C_{p,i}$	heat capacity ($J\,(kg\,K)^{-1}$)
$D_{1,i}$	solid phase diffusivity ($m^2\,s^{-1}$)
$D_{10,i}$	solid phase diffusivity at reference temperature ($m^2\,s^{-1}$)
$E_{a,D,i}$	active energy for diffusion ($kJ\,mol^{-1}$)
$E_{a,k,i}$	reaction active energy ($kJ\,mol^{-1}$)
h	heat transfer coefficient ($W\,m^{-2}\,K^{-1}$)
I	cell current (A)
I_{app}	cell current density based on A_{cell} ($A\,m^{-2}$)
$j_{0,i}$	exchange current density ($A\,m^{-2}$)
$j_{loc,i}$	local current density ($A\,m^{-2}$)
$k_{0,i}$	reaction rate constant ($m^{2.5}mol^{-0.5}s^{-1}$)
k_i	thermal conductivity ($W\,(m\,K)^{-1}$)
L_i	thickness (μm)
Q_{act}	active heat generation ($J\,m^{-3}$)
Q_{ohm}	ohmic heat generation ($J\,m^{-3}$)
Q_{rea}	reaction heat generation ($J\,m^{-3}$)
r	radius distance variable of particle (m)
R_{cell}	total resistance in battery (Ω)
R_i	characteristic radius of electrode particles (μm)
$S_{a,i}$	specific surface area (m^{-1})
$SOC_{0,i}$	initial state of charge
t	time (s)
t_+	transference number of Li ion species dissolved in liquid
T	absolute temperature (K)
T_{amb}	ambient temperature (K)
U_i	thermodynamic, open circuit voltage (V)
ν	thermodynamic factor relating to electrolyte activity
x	distance variable through a cell component (m)
y	dimensionless radial distance of particles
$\bar{x}$	average composition variable of Li in $Li_{\bar{x}}C_6$
$\bar{y}$	average composition variable of Li in $Li_{\bar{y}}Mn_2O_4$

Greek letters

$\alpha_{a,i}$	transfer coefficient for anodic current
$\alpha_{c,i}$	transfer coefficient for cathodic current
$\varepsilon_{1,i}$	active material volume fraction
$\varepsilon_{2,i}$	volume fraction
ϕ_i	electric potential (V)
γ_i	Bruggeman tortuosity exponent
κ	ionic or electronic conductivity ($S\,m^{-1}$)
ρ_i	density ($kg\,m^{-3}$)
σ_i	solid phase conductivity ($S\,m^{-1}$)

Subscripts, superscripts and acronyms

0	initial or equilibrated state
1	solid phase
2	liquid phase
amb	ambient (temperature)
app	current applied to battery
Cell	battery
Ch	charge
Disch	discharge
irr	irreversible
n	negative electrode
p	positive electrode
re	reversible
ref	reference composition of relative to a Li/lithium ion reference electrode or reference temperature for Arrhenius formula
s	separator
surf	surface of active material particles

temperature change are estimated by comparing modeling results with experimental data. Temperature sensitive parameters (such as diffusivity of lithium ion in solid and liquid phase and reaction rate constant) are estimated. After comprehensive model validation at different operating temperatures and charge–discharge rates, the influence of operating temperature on lithium discharge behavior and lithium ion concentration distribution are simulated and discussed. The roles of heat sources/sinks of electrochemical reaction in different operating conditions are analyzed.

2. Experiments

Commercial $LiMn_2O_4$ battery (90 mm × 57 mm × 25 mm prismatic battery, capacity 11.5Ah, LiC_6 anode material, $LiMn_2O_4$ cathode material, 1.2 mol L^{-1} $LiPF_6$ in PC/EC/DMC solvent) is experimentally characterized. A LAND (CT2001-B, China) test system, 8-channel A to D converter and a computer data logger is used to monitor the charge–discharge current and battery voltage. Real-time graph is created and stored in computer. The battery is placed in a temperature control box for being operated at different temperatures.

The full capacity of the battery is measured at 25 °C with following steps: (1) the battery is fully charged to 3.8 V with a constant current of 2 A and with constant voltage at 3.8 V till charge current declined to 200 mA at 25 °C; (2) according to the method declared by the manufacturer. Then, battery is discharged with a constant current of 2 A, down to 2.5 V, the end-of-discharge voltage specified by the battery manufacturer.

The initial OCV of batteries was measured using multimeter with 5.5 digit resolution. The battery is discharged at constant current (0.2C, 0.5C, 1C, 2C) at room temperature (25 °C), so as to characterize the electrochemical behavior of lithium ion battery at normal temperature.

A temperature sensor probe was stuck on the center site of the batteries to monitor the surface temperature change during operation. The batteries were carefully wrapped by thermal insulation material-cotton. Another temperature sensor measured the ambient temperature in situ. Lastly, the batteries were charged and discharged at some constant current (0.2C, 0.5C, 2C) continuously. Between the charging process and discharging process, 10 h were given to let the batteries temperature down to the ambient temperature. During full process, battery surface temperature will be measured and recorded in situ by multi-channel temperature logger. We tried to conduct these experiments in insulating condition so as to eliminate the influence of ambient temperature, however, the experimental condition cannot be ideally insulate, so it is actually a quasi insulating condition with relatively small heat transfer.

Pulse-test at different ambient temperatures (0 °C, 10 °C, 25 °C, 55 °C) and different currents (0.2C, 0.5C, 1C, 2C) are performed to characterize dynamic performance of lithium ion battery. It should be noted that the temperature dependent parameters, such as lithium ion diffusivity in solid and liquid phases and reaction rate can be extracted from these experimental data.

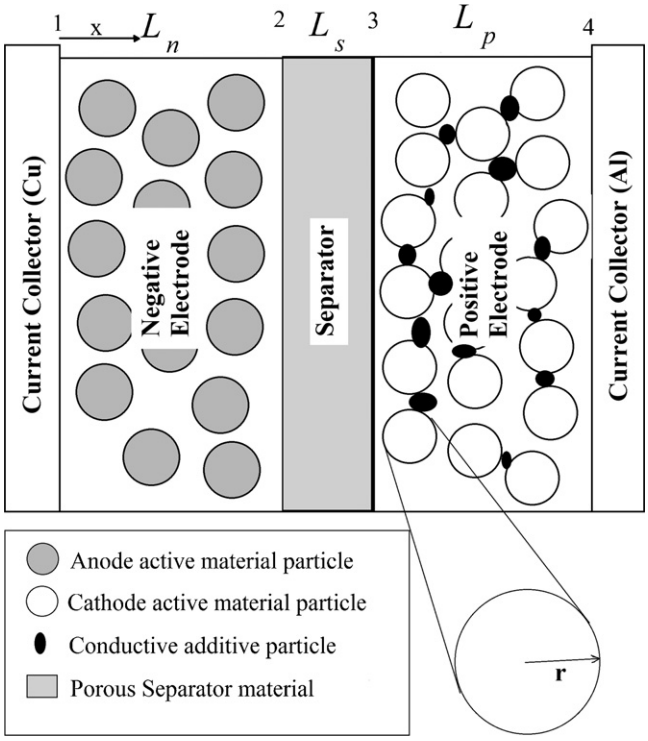

Fig. 1. Schematic of lithium-ion battery calculation domain.

3. Model development

3.1. Model assumptions and calculation domain

The electro-thermal model for $LiMn_2O_4$ lithium ion battery in this paper is developed based on the pseudo two-dimensional model of Doyle et al. [4,7]. The main model assumptions were shown as follows:

(1) Gas generated during operation is neglected, and only liquid phase and solid phase in lithium ion battery are considered.
(2) Side reactions during operation are neglected.
(3) Active materials in solid electrodes are considered to be homogenous, and are composed with spherical particles.
(4) The effects of current collectors on lithium ion transfer and heat transfer are neglected.

Fig. 1 shows a schematic calculation domain of one-dimensional (1D) battery model [4,7,8]. Two inner boundaries (anode/separator interface boundaries 2 and cathode/separator interface boundaries 3) and two external boundaries (anode/current collector interface boundary 1 and cathode/current collector interface boundary 4) are shown in the figure.

3.2. Governing equations

3.2.1. Electronic charge balance

3.2.1.1. Solid phase. Electronic charge balance for solid phase can be expressed as follows:

$$L_i\nabla\cdot\left(-\frac{\kappa_1^{\text{eff}}}{L_i^2}\nabla\phi_1\right) = -L_i S_{a,i} j_{\text{loc},i} \tag{1}$$

$$S_{a,i} = \frac{3\varepsilon_{1,i}}{R_i};\ \kappa_1^{\text{eff}} = \kappa_1\varepsilon_1^{\gamma_1} \tag{2}$$

where ϕ_1 is arbitrarily set at zero at boundary 1; at boundary 4, the charge flux is set to be equal to the average current density of the battery, Eq. (3); at boundary 2 and boundary 3, there is no charge flux, Eq. (4) and the boundary condition is set as isolation

$$\phi_1\big|_{x=0} = 0;\ -\frac{\kappa_1^{\text{eff}}}{L_i^2}\nabla\phi_1\bigg|_{x=L_n+L_s+L_p} = -I_{\text{app}} \tag{3}$$

$$-\frac{\kappa_1^{\text{eff}}}{L_i^2}\nabla\phi_1\bigg|_{x=L_n+L_s} = 0;\quad -\frac{\kappa_1^{\text{eff}}}{L_i^2}\nabla\phi_1\bigg|_{x=L_n} = 0 \tag{4}$$

3.2.1.2. Solution phase. The governing equation for electronic charge balance in solution phase is expressed as

$$\nabla\cdot\left\{\frac{\kappa_2^{\text{eff}}}{L_i}\left[-\nabla\phi_2 + \frac{2RT}{F}\left[1+\frac{\partial\ln f}{\partial\ln c_2}\right](1-t_+)\frac{\nabla c_2}{c_2}\right]\right\} = S_{a,i} j_{\text{loc}} L_i \tag{5}$$

$$\kappa_2^{\text{eff}} = \kappa_2\varepsilon_2^{\gamma_2} \tag{6}$$

Liquid-junction potential is introduced in Eq. (5) with expression

$$K_{\text{junc}} = \frac{2RT}{F}\left[1+\frac{\partial\ln f}{\partial\ln c_2}\right](1-t_+) = \frac{2RT}{F}\nu \tag{7}$$

where ν is the thermodynamic factor relating to electrolyte activity, it is temperature and concentration dependent.

There is no flux at external boundaries (boundary 1 and boundary 4), Eq. (8); φ_2 is taken to be continuous at inner boundaries (boundary 2 and boundary 3).

$$\frac{\partial\phi_2}{\partial x}\bigg|_{x=0} = \frac{\partial\phi_2}{\partial x}\bigg|_{x=L_n+L_s+L_p} = 0 \tag{8}$$

3.2.2. Mass balance

3.2.2.1. Solid phase. The mass balance of lithium ions in an intercalation particle of electrode active material is described by Fick's law. Let the variable y equal to r/R_i, the mass transport within solid phase can be described as

$$y^2 R_i\frac{\mathrm{d}c_{1,i}}{\mathrm{d}t} + \frac{\partial}{\partial y}\left(-y^2\frac{D_{1,i}}{R_i}\frac{\partial}{\partial y}(c_{1.i})\right) = 0 \tag{9}$$

where R_i is the particle radius. The lithium concentration at the surface of the particles, $y=1$, is coupled to the concentration and flux in the 1D model for the charge and material transport in the electrolyte. The flux at the center of sphere, $y=0$, is set to zero, because there is no species source.

3.2.2.2. Solution phase. Solution phase material balance for LiF_6 dissolved in the liquid phase

$$L_i\varepsilon_{2,i}\frac{\mathrm{d}c_2}{\mathrm{d}t} + \nabla\cdot\{-\frac{D_2^{\text{eff}}}{L_i}\nabla c_2\} = \frac{L_i S_{a,i} j_{\text{loc},i}}{F}(1-t_+) \tag{10}$$

$$D_2^{\text{eff}} = D_2\varepsilon_{2,i}^{\gamma_2} \tag{11}$$

The flux of liquid species is set to zero at external boundaries (boundary 1 and boundary 4), liquid species flux and species concentration are taken to be continuous at inner boundaries (boundary 2 and boundary 3).

3.2.3. Electrochemical kinetics

The local current per active material area is calculated using the Bulter–Volmer equation:

$$j_{\text{loc},i} = j_{0,i}\left\{\exp\left(\frac{\alpha_{a,i}\eta_i F}{RT}\right) - \exp\left(\frac{-\alpha_{c,i}\eta_i F}{RT}\right)\right\} \tag{12}$$

where $j_{loc,i}$ is driven by overpotential, η_i, defined as the difference between solid and electrolyte phase potentials minus U, the thermodynamic equilibrium potential of the solid phase.

$$\eta_i = \phi_{1,i} - \phi_{2,i} - U_{ref,i} \tag{13}$$

where the equilibrium potential, U, is taken to be a function of the solid phase lithium ion concentration at the particle surface. In Eq. (14), exchange current density, $j_{0,i}$, acts as a bridge connecting concentrations in both solid phase and liquid phase:

$$j_{0,i} = Fk_i c_2^{\alpha_{a,i}} \left(c_{1,max,i} - c_{1,surf,i}\right)^{\alpha_{a,i}} c_{1,surf,i}^{\alpha_{c,i}} \tag{14}$$

where k_i is a reaction rate, considered temperature dependent in this paper. α_a and α_c are the anodic and cathodic transfer coefficients, respectively.

3.2.4. Energy balance

The following equation governs energy balance in lithium ion battery. There are three parts of heat sources during charge and discharge processes, including reaction heat Q_{rea}, ohmic heat Q_{ohm} and active polarization heat Q_{act}.

$$L_i \rho_i C_{p,i} \frac{\partial T}{\partial t} + \nabla \cdot \left(\frac{-k_i}{L_i} \nabla T\right) = L_i (Q_{rea} + Q_{act} + Q_{ohm}) \tag{15}$$

where active polarization heat is

$$Q_{act} = S_{a,i} j_{loc,i} (\phi_{1,i} - \phi_{2,i} - U_i) \tag{16}$$

Reaction heat is

$$Q_{rea} = S_{a,i} j_{loc,i} T \frac{\partial U_i}{\partial T} \tag{17}$$

Ohmic heat is

$$Q_{ohm} = \frac{\sigma^{eff}}{L_i^2} \nabla\phi_1 \cdot \nabla\phi_1 + \frac{\kappa^{eff}}{L_i^2} \nabla\phi_2 \cdot \nabla\phi_2 + \frac{\kappa_D^{eff}}{L_i^2} \frac{\nabla c_2}{c_2} \cdot \nabla\phi_2 \tag{18}$$

Active heat Q_{act} and ohmic Q_{ohm} are irreversible, while reaction heat Q_{rea} is reversible.

$$Q_{irr} = Q_{act} + Q_{ohm} \tag{19}$$

$$Q_{re} = Q_{rea} \tag{20}$$

The temperature-dependent open circuit potential of electrode i is approximated by Taylor's first order expansion around a reference temperature:

$$U_i = U_{ref,i} + (T - T_{ref}) \frac{dU_i}{dT} \tag{21}$$

where $U_{ref,i}$ is the open circuit potential under the reference temperature.

According to Newton's cooling law, the boundary condition for energy balance is expressed as

$$-\lambda \left.\frac{\partial T}{\partial x}\right|_{x=0} = h(T_{amb} - T); \; -\lambda \left.\frac{\partial T}{\partial x}\right|_{x=L_n+L_s+L_p} = -h(T_{amb} - T) \tag{22}$$

where h is lumped heat transfer coefficient and T_{amb} is the ambient temperature.

3.3. Solution method

The calculations of model were performed using the finite element commercial software COMSOL MULTIPHYSICS® (Version 3.5a). Battery performance was calculated by given battery current. The outputs of the model are the cell potential, current density distribution, species and concentrations distributions. The cell potential is derived by the following expression:

$$E_{cell} = \left.\phi_1\right|_{x=L_n+L_s+L_p} - \left.\phi_1\right|_{x=0} \tag{23}$$

4. Model calibration and validation

4.1. Model calibration

4.1.1. Model parameters

Model parameters are from experimental measurement, literature and estimation. Parameters for an 11.5Ah $LiMn_2O_4$ battery are listed in Table 1, including design specifications, lithium ion concentration parameters, kinetic and transport properties and thermal properties.

4.1.2. Liquid phase parameters

The data of lithium ion diffusivity in solution phase D_2, electric conductivity in solution phase κ_2 and thermodynamic factor ν are adopted from the published literature [9]:

$$D_2 = 1 \times 10^{-4} 10^{-4.43(54.0/(T-229.0-0.05c))-2.2\times10^{-4}c_2} \tag{24}$$

$$\begin{aligned}\kappa_2 = {} & 1 \times 10^{-4} c_2 \big(-10.5 + 0.074T - 6.69 \times 10^{-5} T^2 \\ & + 6.68 \times 10^{-4} c_2 - 1.78 \times 10^{-5} c_2 T + 2.8 \times 10^{-8} c_2 T^2 \\ & + 4.94 \times 10^{-7} c_2^2 - 8.86 \times 10^{-10} c_2^2 T\big)^2\end{aligned} \tag{25}$$

$$\begin{aligned}\nu = {} & 0.601 - 0.24\sqrt{10^{-3} c_2} \\ & + 0.982[1 - 0.0052(T - 294.0)\sqrt{10^{-9} c_2^3}]\end{aligned} \tag{26}$$

Table 1
Model parameter for an 11.5Ah $LiMn_2O_4$ HEV battery.

	Anode	Separator	Cathode
Design specifications (geometry and volume fractions)			
A_{cell} (m^2)		0.4275[a]	
$\varepsilon_{1,i}$	0.5[a]	–	0.49[a]
$\varepsilon_{2,i}$	0.33[a]	0.54[a]	0.332[a]
L_i (μm)	120[a]	30[a]	150[a]
R_i (μm)	12.5[a]	–	8.5[a]
Lithium ion concentrations			
$C_{2,0}$ (mol m^{-3})		1200[a]	
$C_{max,i}$ (mol m^{-3})	26 390[b]	–	22 860[b]
$SOC_{0,i}$	0.74[c]	–	0.35[c]
Kinetic and transport properties			
$\alpha_{a,i}$, $\alpha_{c,i}$	0.5	–	0.5
γ_i	1.5	4[d]	1.5
D_2 (m^2 s^{-1})		Eq. (24)	
$D_{10,i}$ (m^2 s^{-1})	3.9×10^{-14}[b]	–	7.51×10^{-14}[d]
$E_{a,D,i}$ (kJ mol^{-1})	35[e]	–	31.556[d]
$k_{0,i}$ ($m^{2.5}$ $mol^{-0.5}$ s^{-1})	1.764×10^{-11}[f]	–	3.626×10^{-11}[d]
$E_{a,k,i}$ (kJ mol^{-1})	20[c]	–	32.694[d]
κ_1 (S m^{-1})	100[b]	–	3.8[b]
κ_2 (S m^{-1})		Eq. (25)	
t^+		0.363[b]	
ν		Eq. (26)	
F (C mol^{-1})		96 487	
Thermal properties			
k_i (W (m K)$^{-1}$)	1.04[g]	1[g]	1.48[g]
ρ_i (kg m^{-3})	2500[h]	1200[h]	1500[h]
Cp_i (J (kg K)$^{-1}$)	700[h]	700[h]	700[h]
T_{ref} (K)		298.15	

[a] Battery manufacturer.
[b] Ref. [9].
[c] Ref. [10].
[d] Estimated.
[e] Ref. [11].
[f] Ref. [6].
[g] Ref.[12].
[h] Ref. [13].

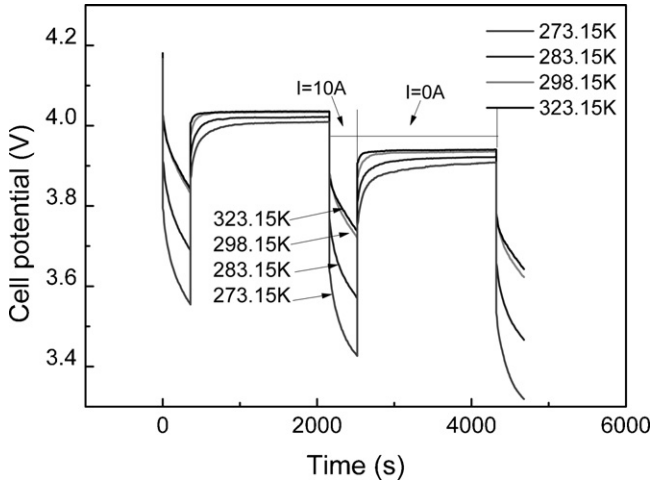

Fig. 2. Experimental data of 1C pulse test at different temperatures.

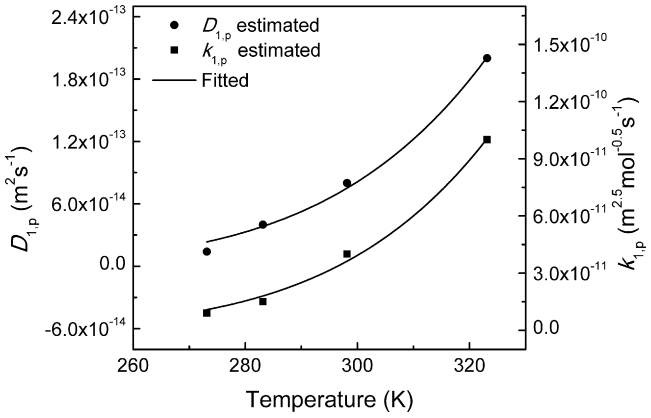

Fig. 4. Estimated parameters D_p and k_p are fitted into Arrihenius formula.

4.1.3. Kinetic and transport properties

Both diffusivity coefficient and reaction rate constants are fitted into the following Arrhenius formula [10]:

$$A_i = A_{0,i} \exp\left(\frac{E_{a,i}}{R}\left(\frac{1}{T_{\text{ref}}} - \frac{1}{T}\right)\right) \tag{27}$$

$$D_{1,\text{n}} = 3.9 \times 10^{-14} \exp\left(\frac{35000}{R}\left(\frac{1}{298.15} - \frac{1}{T}\right)\right) \tag{28}$$

where $D_{1,\text{n}}$ and $k_{1,\text{n}}$ data for MCMB negative electrode come from the literature as shown in Table 1. Battery pulse test performance, as shown in Fig. 2, varies at different temperatures, mainly due to the variation of $D_{1,\text{p}}$ and $k_{1,\text{p}}$ at different temperatures. The reason may be discussed later. Regarding to this property, $D_{1,\text{p}}$ and $k_{1,\text{p}}$ are estimated and fitted in Arrhenius formula by comparing model simulated data with experimental data. The results are presented in Figs. 3 and 4.

4.1.4. Lumped heat transfer coefficient

Lumped heat transfer coefficient h is determined by comparing experimental data with simulated result (Fig. 5) . Lithium ion battery is discharged with 2C constant current with temperature rising to 50 °C at the end of discharge. Then the current is cut off for temperature relaxation to room temperature. By comparing

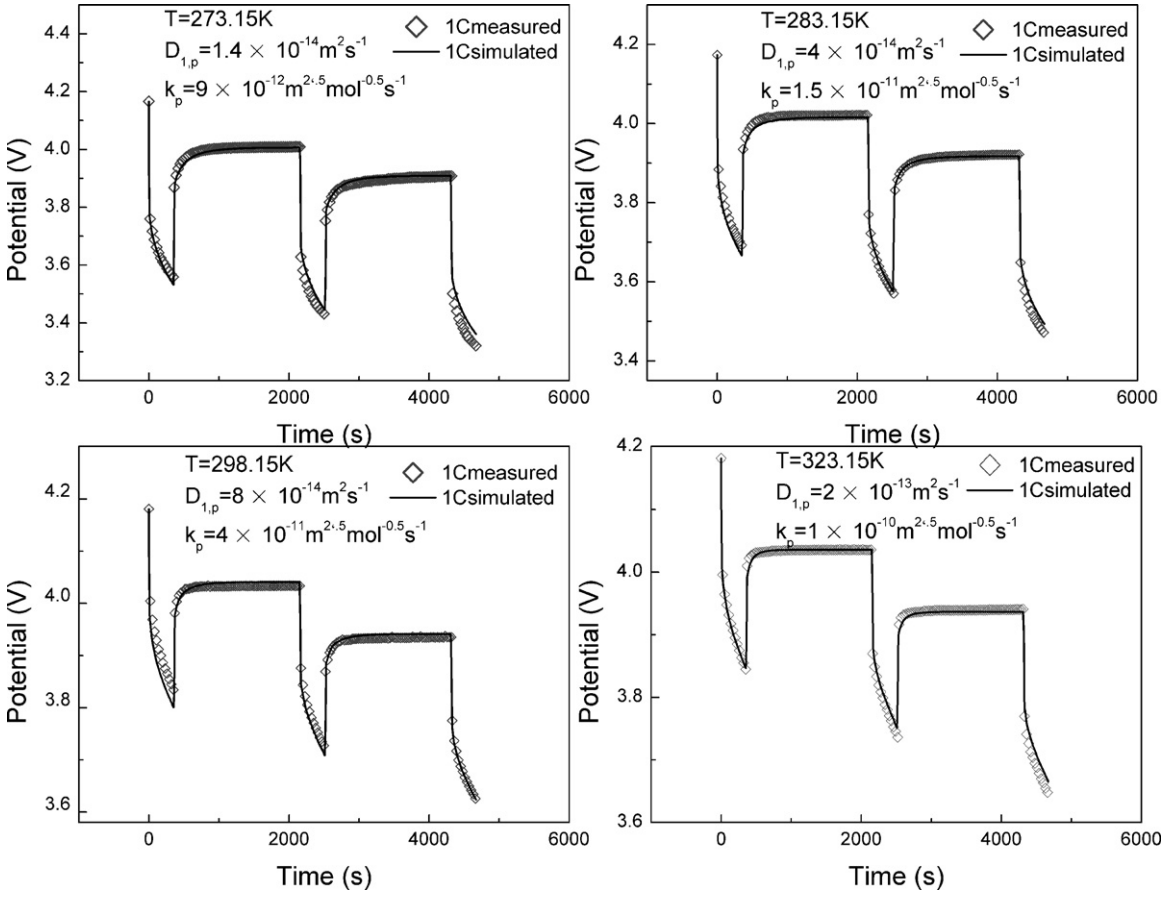

Fig. 3. Estimated parameters D_p and k_p by comparing 1C pulse test experiment data with simulated data.

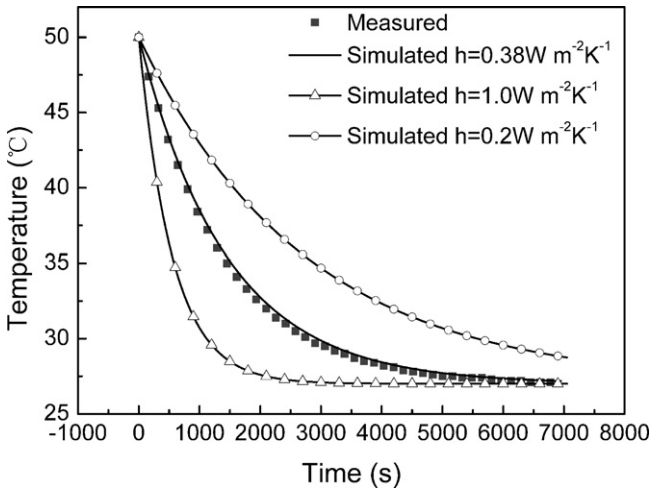

Fig. 5. Determination of lumped heat transfer coefficient h by comparing experimental data with simulated results.

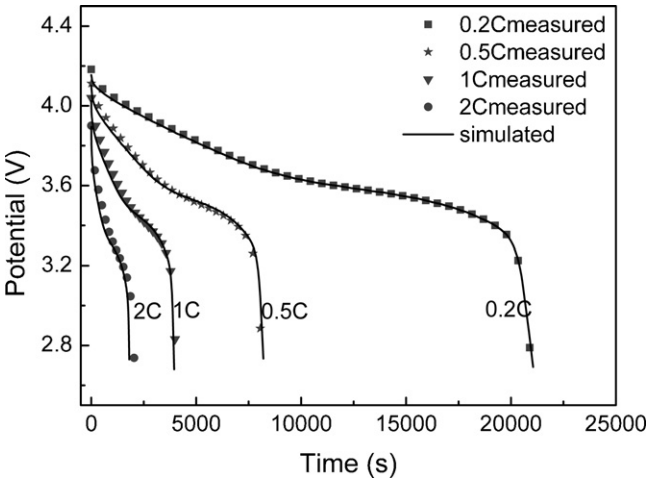

Fig. 8. Comparison of simulated results with experimental data at constant currents (0.2C, 0.5C, 1C, 2C) at constant temperature 25 °C.

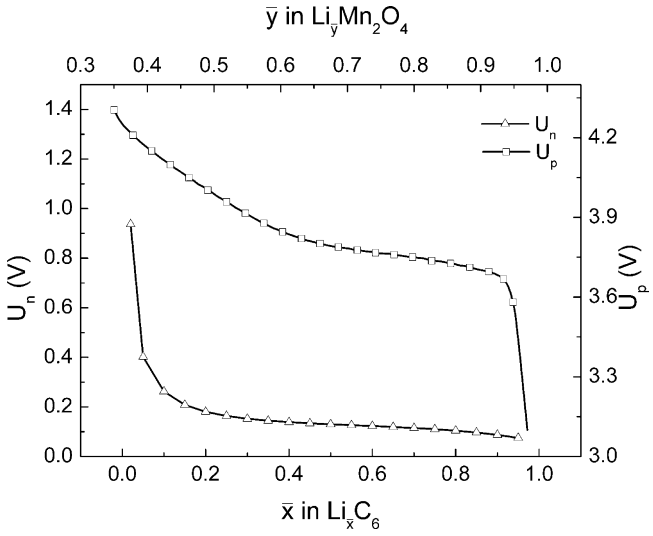

Fig. 6. Open circuit voltage of negative electrode U_n and positive electrode U_p.

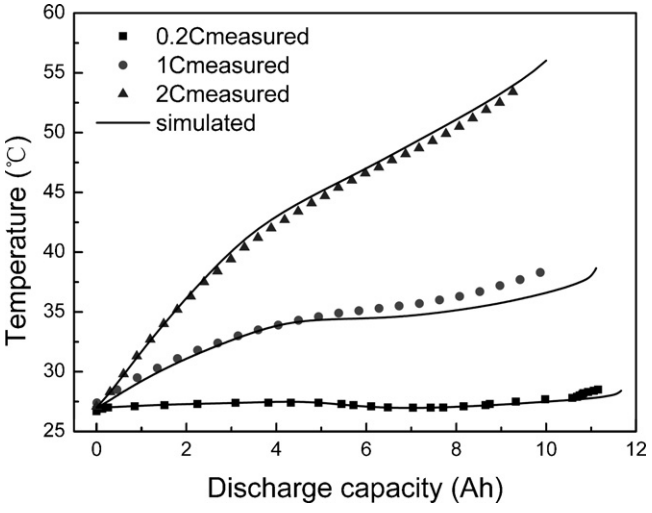

Fig. 9. Comparison of simulated results of battery surface temperature with expreimental data during quasi insulating discharge (0.2C, 1C, 2C).

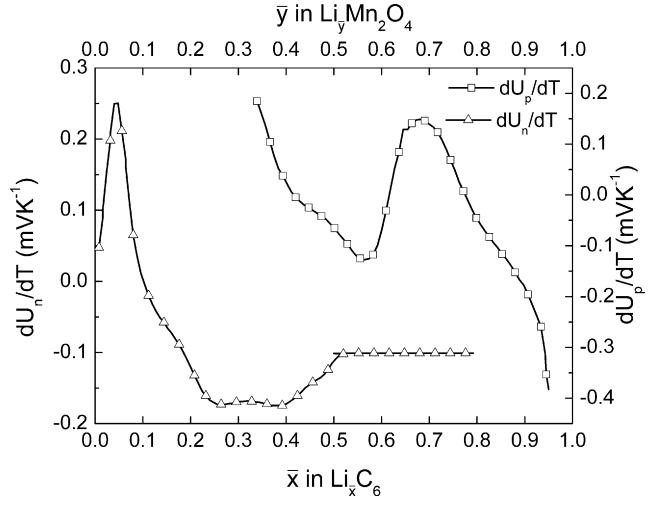

Fig. 7. Entropy change of negative electrode dU_n/dT and positive electrode dU_p/dT as a function of state of charge.

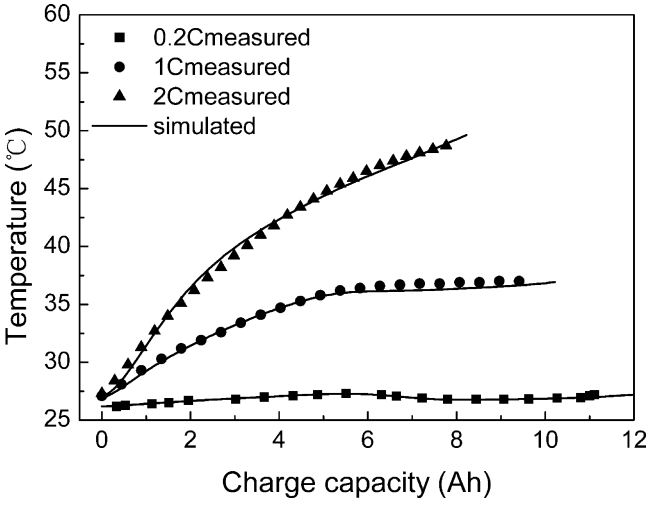

Fig. 10. Comparison of simulated results of battery surface temperature with expreimental data during quasi insulating charge (0.2C, 1C, 2C).

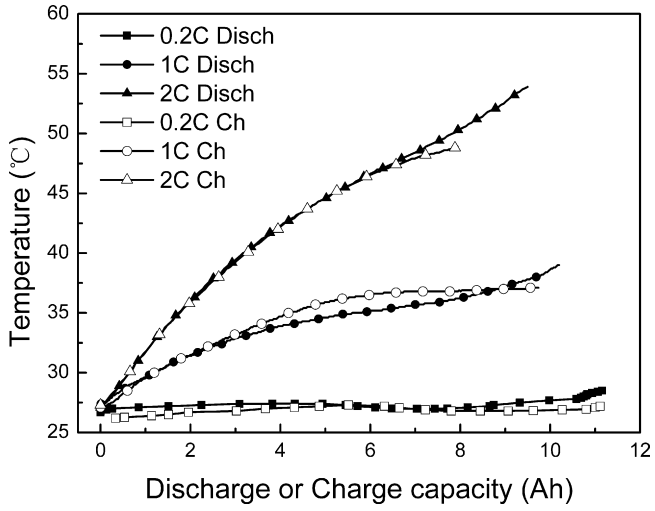

Fig. 11. Comparison of measured surface temperature between quasi-insulating charge and discharge.

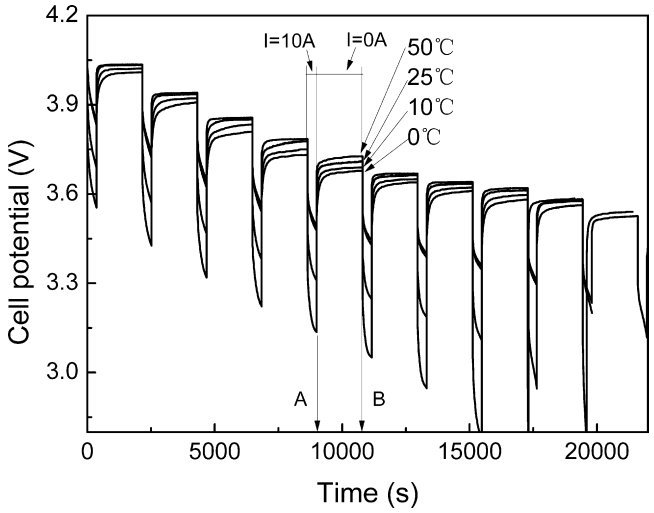

Fig. 12. Experimental data of 1C pulse test at different temperatures.

temperature relaxation curve, we determine the heat transfer coefficient to be 0.38 $W(m^{-2}K^{-1})$. Lumped heat transfer coefficient here represents the synthetically effect of heat conduction, convection heat transfer and radiative heat transfer.

4.1.5. Electrode thermodynamic properties

As shown in Fig. 6, open circuit voltage (OCV) of positive electrode (U_p) is experimentally (LAND battery test system, China) measured using method present in Ref. [11]; open circuit voltage (OCV) of negative electrode (U_n) comes from Ref. [12]. In Fig. 7, entropy change in positive electrode is $\Delta S_p = nF(dU_p/dT)$, dU_p/dT is calculated from data of Ref. [13] using method presented in Ref. [14]; negative electrode entropy change is $\Delta S_n = nF(dU_n/dT)$, dU_n/dT data comes from Ref. [6].

State of charge of both negative and positive electrodes has the same expression as follows:

$$SOC_i = \frac{c_{1,i}}{c_{1,\max,i}} \tag{29}$$

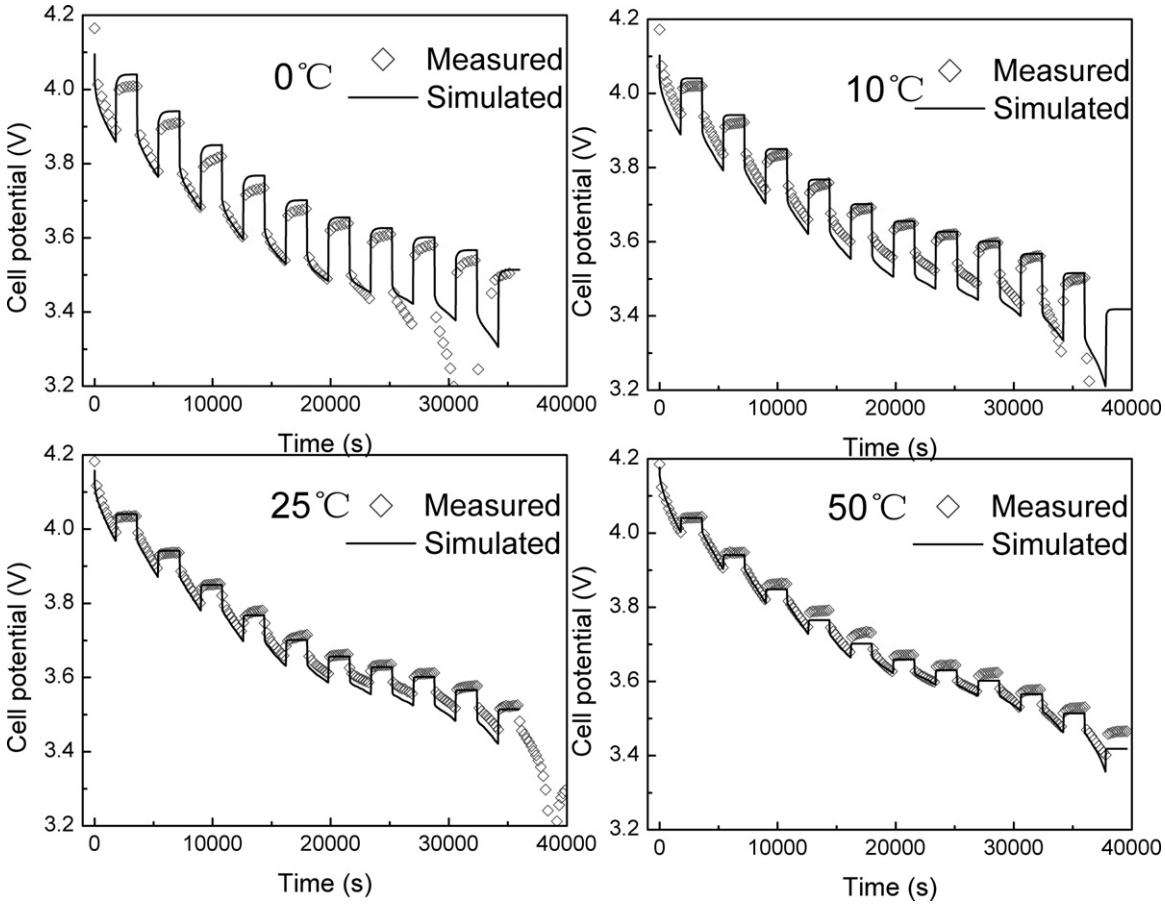

Fig. 13. 0.2C pulse test validation by comparing experiment data with simulated results.

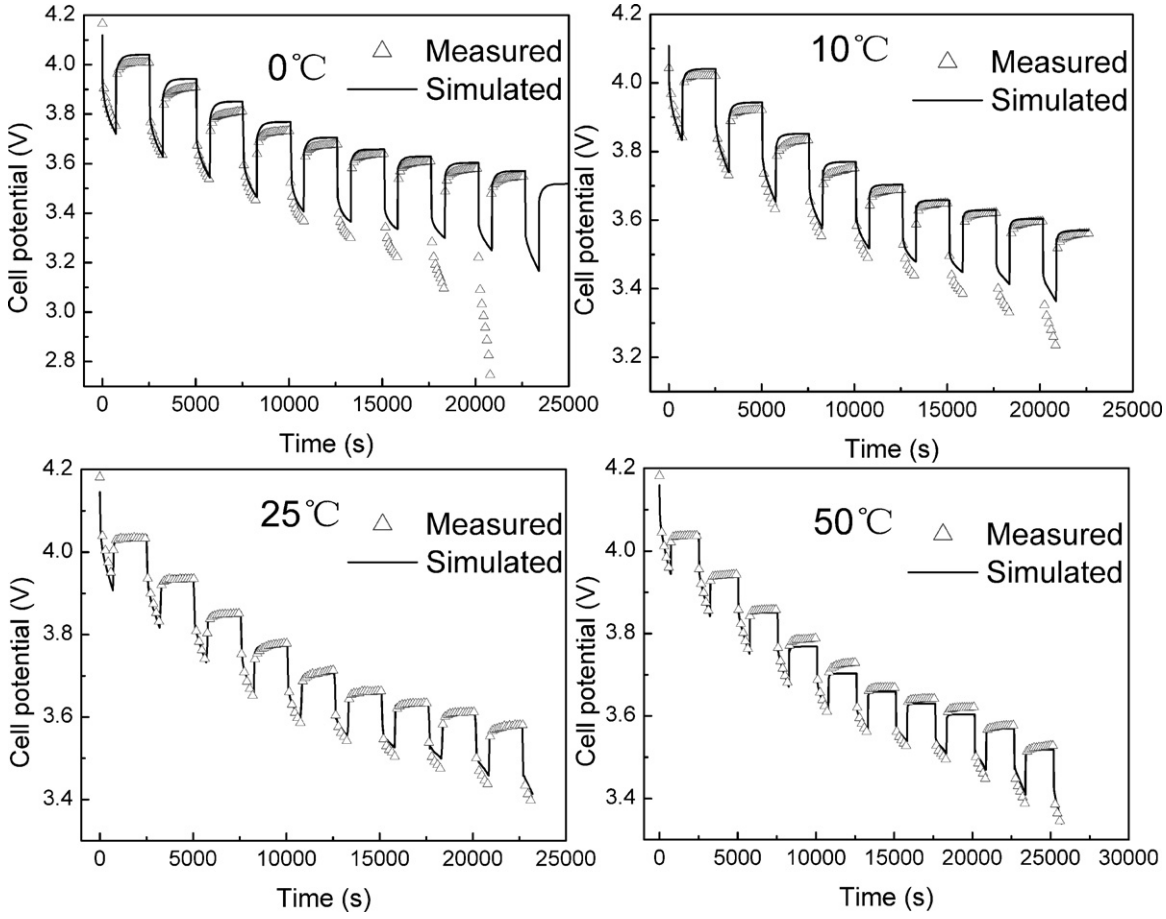

Fig. 14. 0.5C pulse test validation by comparing experiment data with simulated results.

That is $SOC_n = \bar{x} = c_{1,n}/c_{1,max,n}$ in $Li_{\bar{x}}C_6$ and $SOC_p = \bar{y} = c_{1,p}/c_{1,max,p}$ in $Li_{\bar{y}}Mn_2O_4$. Data of U_p, U_n, dU_n/dT and dU_p/dT are fitted as functions of SOC by piecewise cubic method in FUNCTION dialog box of COMSOL.

4.2. Model validation

Model validation is conducted by comparing simulated results with experiment data at different conditions. This model is validated from three aspects: electrochemically, thermally and electrochemical-thermally.

4.2.1. Discharge behavior at constant temperature condition

Fig. 8 shows the comparison between simulated results and experimental data during discharge under the operating condition at constant current discharge (0.2C, 0.5C, 1C, 2C) at constant temperature (25 °C). The results indicated that the modeling results agreed well with the experimental results with the maximum error less than 2%.

4.2.2. Heat sources and surface temperature

Fig. 9 shows comparison of simulated results against experimental data of battery surface temperature during discharging process in quasi insulating condition. It can be seen that the modeling results of battery surface temperature at both 0.2C and 2C discharging agreed well with the experimental results, while there is a little larger deviation at the end of 1C discharge curve. The results indicate that the battery temperature rise faster with larger discharging current. When the discharge current is large, the temperature increase fast. For example, when discharging at 2C discharge current, the temperature increase about 30 °C from the beginning at discharging process to the end of the discharging process. In this situation, the battery cooling system must be carefully designed to avoid the battery safety problem. It also can be seen obviously that the battery surface temperature rise faster at the beginning of discharging process, while rise slower when the discharge capacity is larger than about 6Ah (half of the full battery capacity). When at the beginning of the discharging process, the temperature is relatively lower, the battery polarization is relatively larger, thus the more heat generated during this period. In addition, the lumped heat transfer is less during the beginning of discharging since the temperature difference between the battery surface and environment is relatively small.

Fig. 10 also shows good agreement of temperature between simulation and experiment during charging (0.2C, 1C, 2C). We find that surface temperature change during charging and discharging are almost the same, see Fig. 11, which means that the amount of heat generated in battery during low rate (0.2C, 1C, 2C) charging and discharging are almost the same value. We will further discuss heat generation during higher rate charging and discharging below.

4.2.3. Dynamic performance

Fig. 12 shows experimental data for pulse test with 1C current at different temperatures. During one cycle of discharge, the battery is first discharged with 10 A constant current for 360 s and then cut off the current for relaxation for 1800 s. The battery is discharged with this repeating process until cell potential drops to 2.5 V. During the discharge period, there is significant cell potential drop, there are several reasons account for this phenomenon. First, OCV of battery decrease in the discharge process. Then, over potential,

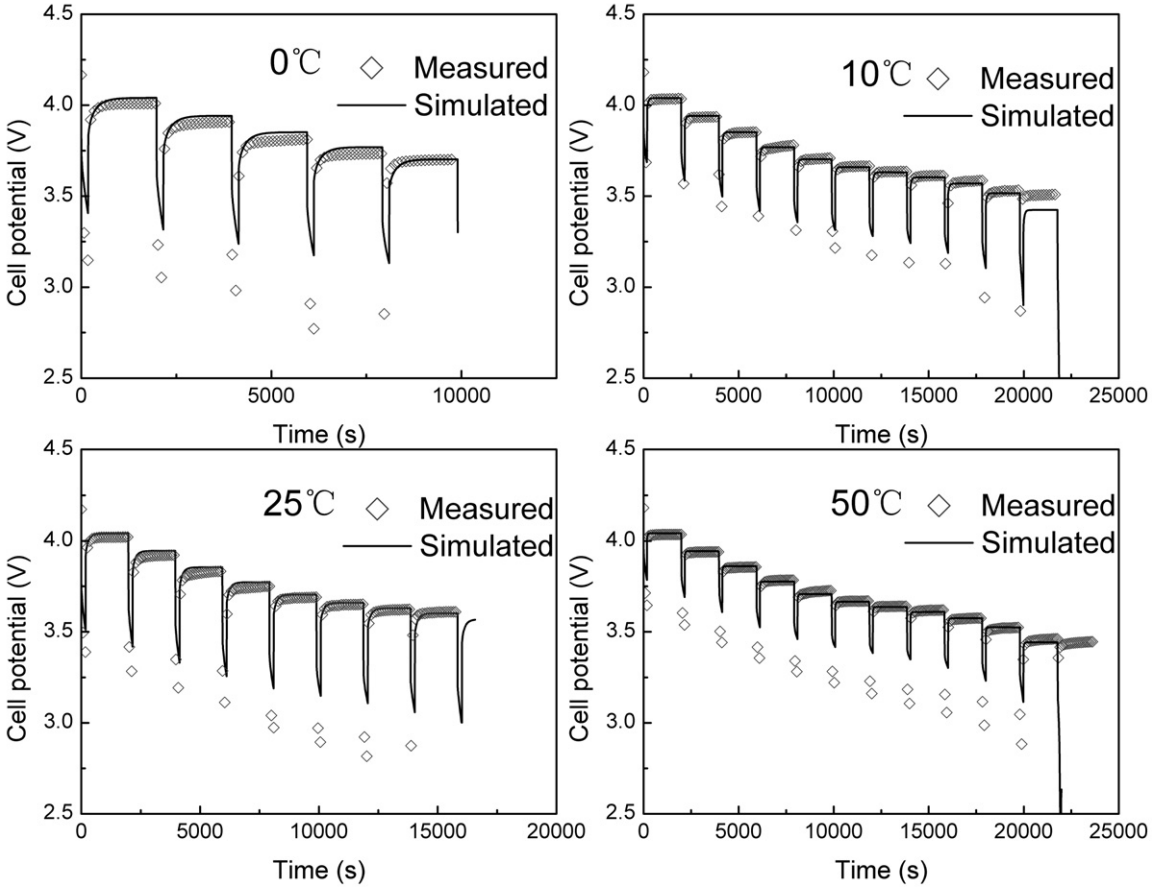

Fig. 15. 2C pulse test validation by comparing experiment data with simulated results.

consisted of concentration polarization, ohmic potential drop and active polarization, accounts for the increasing gap between cell potential and OCV of battery. At point A, we can see that cell potential drop increases with the temperature drop, due to lower lithium ion diffusivity in both solid and liquid phases, larger resistance in battery and lower reaction rate at low temperature. During relaxation period, A–B, active polarization and ohmic potential drop extinct and result in sharp increase of cell potential. Then the concentration polarization takes charge and leads to slower increase of cell potential until B spot. After 1800 s relaxation, cell potential at B spot is approximately the same as OCV of the battery. Cell potentials at point B increase as temperature increases, and this phenomenon results from the entropy change, see Eq. (21). It should be noticed that entropy change is not always the same at different SOC (state of charge) of battery, so the OCV regulation may not necessarily applicable for other SOC.

Parameters related to cell dynamic response and pulse relaxation behavior (e.g. $D_{1,p}$, $k_{1,p}$) are mainly estimated by comparing simulated results with experimental data at 1C discharge at different temperatures (0 °C, 10 °C, 25 °C, 55 °C), the simulated results for pulse test (0.2C, 0.5C, 2C) at different temperatures (0 °C, 10 °C, 25 °C, 55 °C) were validated by experimental results to further check the model applicability.

Figs. 13–15 show the validation results at 0.2C, 0.5C and 2C rates at different temperatures (0 °C, 10 °C, 25 °C, 50 °C). The results shown that the modeling results agreed well with the experimental results, while have a little larger deviations at the end of pulse-test at each temperatures. The deviations are preliminary deduced to be due to the changes of the SEI resistance and contact resistance with temperature or battery state of charge [15,16] which were assumed as constants (zero) in our model.

5. Results and discussion

5.1. Dynamic response of lithium ion concentration in solid phase

One of the potential application fields of the proposed model is to predict the lithium ion concentration distributions within battery electrode and electrolyte, which is helpful for battery design and performance optimizations. As an example, pulse test with 2C discharge rate was chosen to show the lithium ion concentration distribution response. During experimental operation, the battery is discharged at 2C constant current during 0–180 s and then is relaxed by cutting off current during 180–1000 s. One electrode particle at boundary 1 was chosen to examine the lithium ion concentration dynamic change at different positions in radius direction (Fig. 16). At 0–180 s, the lithium ion concentration gradient increases with discharge time, lithium ion concentration at $r/R_n = 0$, 0.2, 0.4 decrease during 0–1000 s, while lithium ion concentration at $r/R_n = 0.6$, 0.8, 1 decrease during 0–180 s and increase during 180–1000 s. Large concentration gradient in solid particles may lead to decrease of battery capacity and battery power during discharging, which will be discussed below. Reducing particle radius and increasing lithium ion diffusivity in solid phase would increase the relaxation performance of battery regarding to the relaxation time factor r^2/D, which is introduced in Ref. [11].

5.2. Effect of temperature on lithium ion distribution

Fig. 17 shows lithium ion concentration distribution across the cell in liquid phase in 20 A (2C) pulse tests ($t = 180$ s). During discharge process, lithium ion concentration in negative electrode is higher than initial concentration and lithium ion concentration in

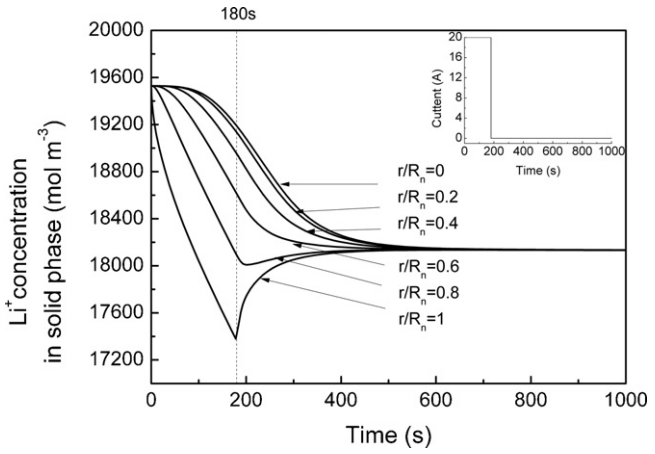

Fig. 16. Lithium ion concentration distribution along particle radius during pulse tests.

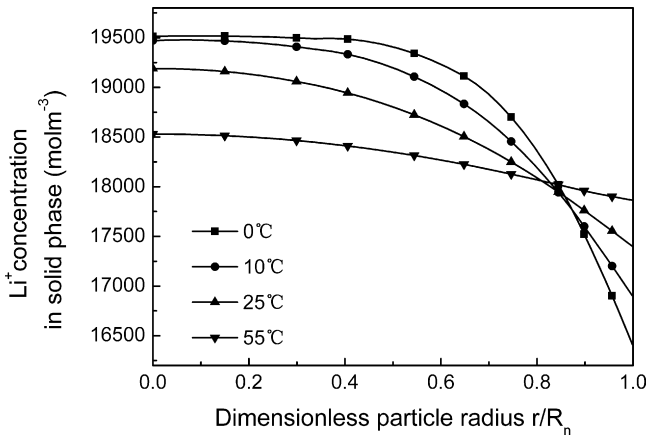

Fig. 18. Lithium ion concentration in solid phase along particle radius at different operating temperatures.

positive electrode is lower than initial concentration. Since lithium ion is extracted from negative electrode and diffuses to liquid phase, lithium ions intercalate to positive electrode particles and lower the liquid phase lithium ion concentration. The lithium ion concentration gradient increases with decrease in operating temperature. This is mainly because that lithium ion diffusivity increases with the operating temperature.

Fig. 18 shows the solid phase lithium ion concentration distribution within a particle at current collector/anode interface. The lithium ion concentration gradient in particle radius direction increases as the operating temperature decrease.

After discussing the lithium ion concentration gradient in both solid and liquid phases upon different temperatures, we further investigate the battery performance variation due to temperature change (Fig. 19). In the electro-thermal model, the discharge current is set to 20 A, and battery is discharged at different temperatures. Battery capacity (product of discharge time and discharge current) decreases significantly with temperature drop, mainly due to large concentration gradient in both solid and liquid phases as discussed above. Battery power (integral of $I \times V \times t$) also decreases sharply with temperature drop. So it is necessary to develop less temperature-dependent electrolyte and electrode materials to improve battery performance at lower temperature, since high performance of battery at low temperature is required for winter use in the application of EV/HEV.

5.3. Reversible heat generation and irreversible heat generation

In this section, the effect of entropy change during charge–discharge on battery temperature change was studied. As mentioned above in Eqs. (19) and (20), heat generation can be divided into reversible heat Q_{re} and irreversible heat Q_{irr}. Influence of current applied to battery on Q_{re} and Q_{irr} is approximated as follows:

$$\frac{Q_{irr}}{Q_{re}} = \frac{Q_{act} + Q_{ohm}}{Q_{rea}} \approx \frac{I^2 R_{cell}}{IT(dU/dT)} \approx I\frac{R_{cell}}{T(dU/dT)} \quad (30)$$

where T does not change significantly during discharging process, dU/dT is a function of state of charge but do not change with current I, and R_{cell} is supposed to be constant, so Q_{re} and Q_{irr} are dominated by dU/dT and R_{cell}, respectively. As shown in Eq. (30), Q_{irr}/Q_{re} is proportion to I. Fig. 18 depicts different parts of heat generated during charge–discharge at 0.2C rate. Irreversible heat Q_{irr} and reversible heat Q_{irr} are of the same order. Q_{irr} is approximately constant with discharge capacity, while Q_{irr} changes with discharge capacity significantly. As a result, the battery surface temperature curves are of the same shape of reversible heat Q_{re} in charge and discharge processes, respectively, see Figs. 20 and 21.

Figs. 22 and 23 present different heat sources (reaction heat Q_{rea}, ohmic heat Q_{ohm}, active polarization heat Q_{act}) during 0.2C and 2C rate discharge. Irreversible heat (Q_{hom} and Q_{act}) in 2C discharge

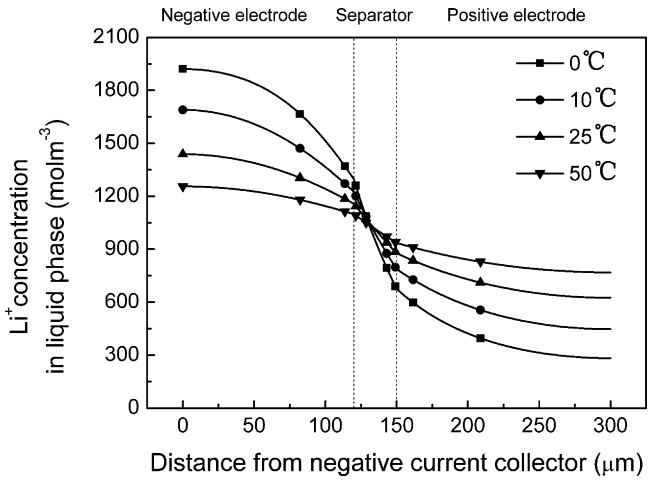

Fig. 17. Lithium ion concentration distribution within liquid phase across the cell at different operation temperatures.

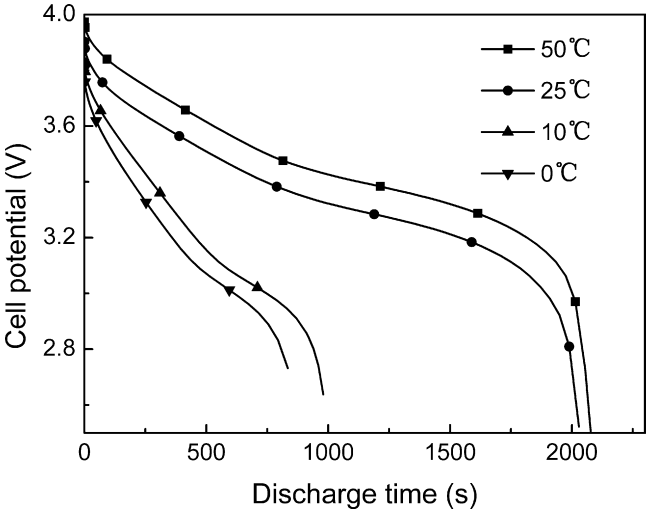

Fig. 19. Influence of temperature on battery 2C discharge performance.

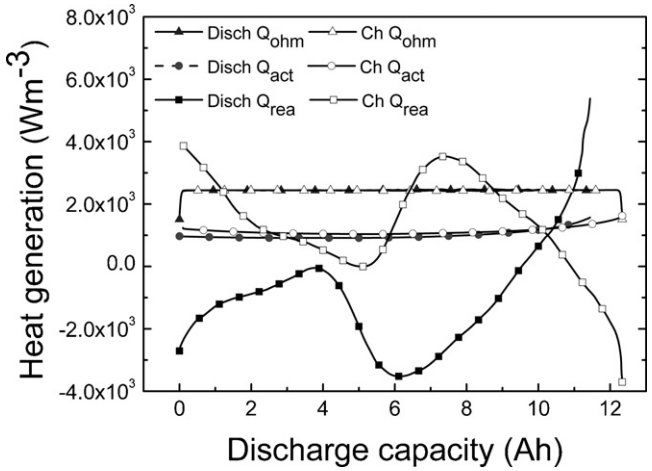

Fig. 20. Different parts of heat generation in lithium ion battery during 0.2C charge–discharge.

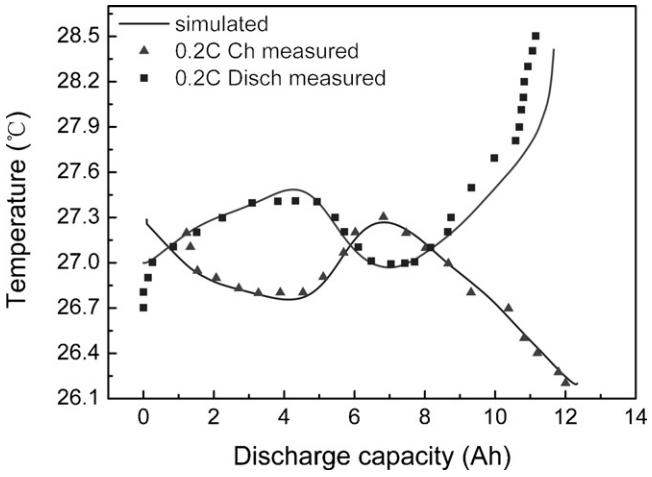

Fig. 21. Simulated and experimental data of battery surface temperature at 0.2C charge–discharge rate.

is approximately 100 times that of 0.2C discharge, and reversible heat (Q_{rea}) in 2C discharge is approximately 10 times that of 0.2C discharge, this phenomenon fit Eq. (30) quite well. Reversible heat and irreversible heat are of the same order during 0.2C discharge, while irreversible heat is about 10 times that of reversible heat during 2C discharge, based on this phenomenon and Eq. (30), we

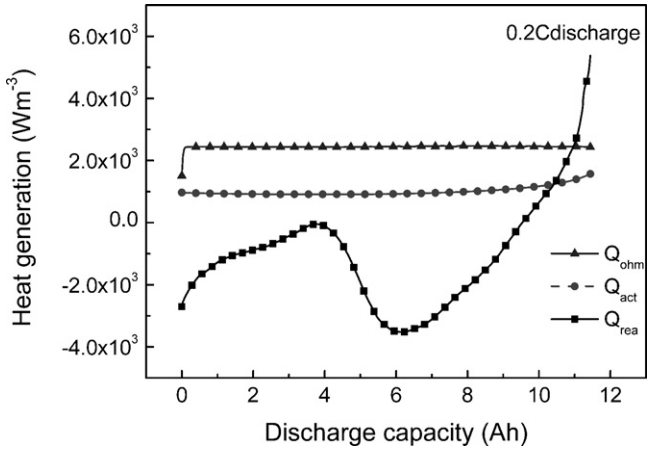

Fig. 22. Different heat sources during 0.2C discharge.

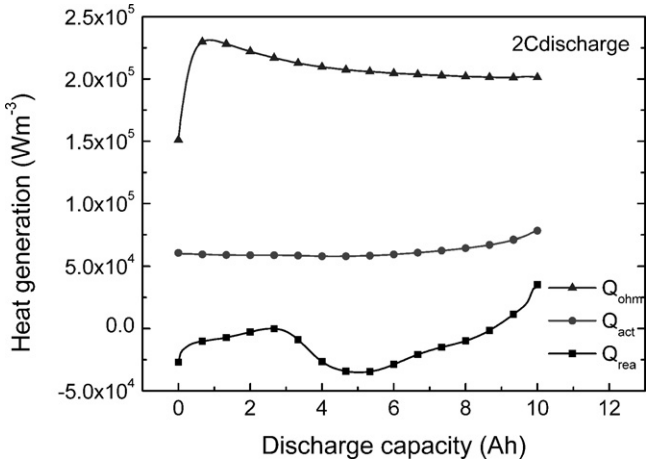

Fig. 23. Different heat sources during 2C discharge.

can safely conclude that reversible heat dominant at low rate discharge and irreversible heat dominant at high rate discharge, and we can ignore reversible heat at high rate (such as 10C) discharge for simplification.

5.4. Simulation of temperature during high rat charge and discharge

In Fig. 24, simulation results of high rate (5C, 7C, 10C) charge–discharge are shown. We consider the battery is charged/discharged with proper cooling condition with a boundary condition of $h = 10\,W\,m^{-2}K^{-1}$, each temperature curve rises at the beginning of charging/discharging, and then reaches equilibrium, the same as Fig. 9 shows. Different from Fig. 11, Fig. 24 shows that equilibrium temperature during charging is higher than that of during discharging, indicating that there would be more heat generated during charging than discharging at higher C rate. It should also be noted that temperature rises up to 70 °C at the end of 10C charging/discharging, this temperature would be harmful for battery and could be dangerous. More intensive cooling measure should be taken for cooling the battery during high rate charge–discharge.

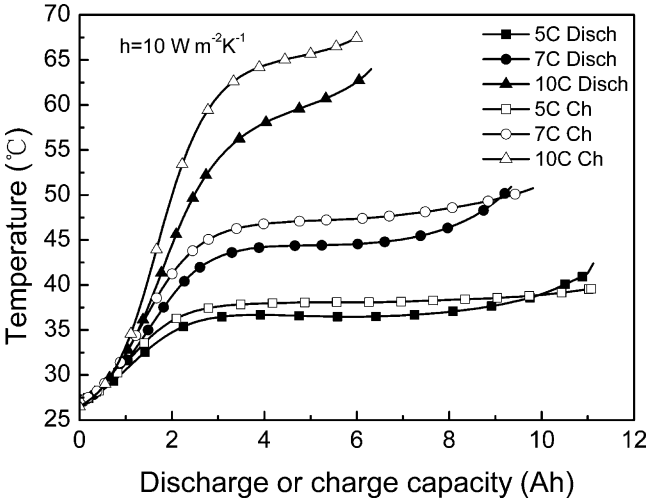

Fig. 24. Simulation results on temperature change during high rate charge and discharge.

6. Conclusions

In this study, a mathematical model by coupling electronic conduction, mass transfer, energy balance and electrochemical mechanism is developed. Lithium ion diffusivity and chemical reaction rate of cathode material are estimated by comparing simulated results with experimental data of pulse test at various current charge–discharge rates (0.2C, 0.5C, 1C, 2C) and operating temperatures (0 °C, 10 °C, 25 °C, 55 °C). The modeling results are further validated in aspects of electrochemical performance, thermal performance and electrochemical-thermal coupling effects, which show good agreement between the modeling results and experimental results.

The modeling results indicated that the lithium ion concentration gradient in both liquid phase and solid phase are greatly affected by temperature variation. The results also indicated that the lithium ion concentration gradient increases when the operating temperature decreases. The above phenomenon results in the capacity losses and power losses of lithium ion battery during low temperature operation. Then, the influence of reversible heat on battery discharge is evaluated. Reversible heat is found to be dominant heat source during low rate discharge and is considered to be negligible for model simplification during high rate discharge. Temperature change during high rate charging/discharging would be too high for battery, proper cooling methodologies should be taken.

References

[1] X.W. Zhang, Electrochim. Acta 56 (2011) 1246–1255.
[2] C.R. Pals, J. Newman, J. Electrochem. Soc. 142 (1995) 3274–3281.
[3] C.R. Pals, J. Newman, J. Electrochem. Soc. 142 (1995) 3282–3288.
[4] M. Doyle, T.F. Fuller, J. Newman, J. Electrochem. Soc. 140 (1993) 1526–1533.
[5] W.B. Gu, C.Y. Wang, J. Electrochem. Soc. 147 (2000) 2910–2922.
[6] K. Kumaresan, G. Sikha, R.E. White, J. Electrochem. Soc. 155 (2008) A164–A171.
[7] T.F. Fuller, M. Doyle, J. Newman, J. Electrochem. Soc. 141 (1994) 1–10.
[8] K.A. Smith, C.D. Rahn, C.Y. Wang, IEEE T. Contr. Syst. T. 18 (2010) 654–663.
[9] L.O. Valoen, J.N. Reimers, J. Electrochem. Soc. 152 (2005) A882–A891.
[10] D. Bernardi, E. Pawlikowski, J. Newman, J. Electrochem. Soc. 132 (1985) 5–12.
[11] D.M. Bernardi, J.Y. Go, J. Power Sources 196 (2011) 412–427.
[12] P. Arora, M. Doyle, R.E. White, J. Electrochem. Soc. 146 (1999) 3543–3553.
[13] H.J. Bang, H. Yang, Y.K. Sun, J. Prakash, J. Electrochem. Soc. 152 (2005) A421–A428.
[14] Q. Huang, M.M. Yan, Z.Y. Jiang, J. Power Sources 156 (2006) 541–546.
[15] K. Onda, T. Ohshima, M. Nakayama, K. Fukuda, T. Araki, J. Power Sources 158 (2006) 535–542.
[16] M. Guo, G. Sikha, R.E. White, J. Electrochem. Soc. 158 (2011) A122–A132.